A Dynamic Consensus Algorithm to Adjust Virtual Impedance Loops for Discharge Rate Balancing of AC Microgrid Energy Storage Units

Guan, Yajuan; Meng, Lexuan; Li, Chendan; Quintero, Juan Carlos Vasquez; Guerrero, Josep M.

Published in:
I E E E Transactions on Smart Grid

DOI (link to publication from Publisher):
10.1109/TSG.2017.2672882

Publication date:
2018

Document Version
Accepted author manuscript, peer reviewed version

A Dynamic Consensus Algorithm to Adjust Virtual Impedance Loops for Discharge Rate Balancing of AC Microgrid Energy Storage Units

Yajuan Guan, *Member, IEEE,* Lexuan Meng, *Member, IEEE,* Chendan Li, *Student Member, IEEE,* Juan C. Vasquez, *Senior Member, IEEE,* and Josep M. Guerrero, *Fellow, IEEE*

***Abstract*— A dynamic consensus algorithm (DCA)-based coordinated secondary control with an autonomous current-sharing control strategy is proposed in this paper for balancing the discharge rate of energy storage systems (ESSs) in an islanded AC microgrid. The DCA is applied for information sharing between distributed generation (DG) units to regulate the output power of DGs according to the ESS capacities and state-of-charge (SoC). Power regulation is achieved by adjusting the virtual resistances of voltage-controlled inverters with an autonomous current-sharing controller. Compared with existing methods, the proposed approach can provide higher system reliability, expandability, and flexibility due to its distributed control architecture. The proposed controller can effectively prevent operation failure caused by over-current and unintentional outage of DGs by means of balanced discharge rate control. It can also provide fast response and accurate current sharing performance. A generalizable linearized state-space model for *n*-DG network in the *z*-domain is also derived and proposed in this paper; the model includes electrical, controller, and communication parts. The system stability and parameter sensitivity have been analyzed based on this model. To verify the effectiveness of the proposed control approach, this study presents simulation results from a ten-node network and a comparison between experimental results obtained from the conventional power sharing control and the DCA-based SoC coordinated control in a setup with three 2.2 kW DG units.**

***Index Terms*— coordinated secondary control, dynamic consensus algorithm, energy storage units, balanced discharge rate, AC microgrids**

I. Introduction

Microgrids (MGs) are considered promising electric power systems with a decentralized power architecture, which supports a flexible electric grid by enabling the integration of renewable energy sources (RESs), energy storage systems (ESSs), and demand response [1]-[3].

A MG should supply power to critical loads without the support of a utility grid and overcome the intermittent nature of RESs. Thus, ESSs are needed in the case of grid-fault, energy-shortage, and load fluctuations. More than one set of distributed ESSs should be equipped for providing redundancy to enhance the system stability and reliability [4], [5]. Therefore, coordinated control is required to guarantee the stored energy balance among ESSs, thereby avoiding deep-discharge and over-charge.

The control capability of an ESS is limited to its energy capacity. The available electrical energy from ESSs is affected by various factors, such as charging conditions, ambient temperature, the charging and discharging currents, and aging [6]. The valve-regulated lead acid (VRLA) battery is as assumed to be a power source for the ESS in this case. The depth of discharge of a VRLA battery exponentially decreases with its lifecycle increases [6]. Hence, state-of-charge (SoC) usually has a limitation to prevent deep-discharge. Moreover, the capacity of a VRLA battery exponentially declines with the increasing discharge current [6], [7]. The total available electrical energy in VRLA batteries is variable according to discharge condition even when the batteries have the same initial SoC values. The conventional coordinated control strategies mainly focus on equal power sharing among distributed generation (DG) units [2], [3]. However, the ESSs in different DG units may have different discharge rates according to their SoC and capacities. The powerless DG will initially be shut down when its SoC is below the threshold; the remaining DGs have to supply more power to the total loads. This situation may produce an overcurrent and unintentional outages, as well as degrade the MG stability and reliability.

To avoid operation failure, all aspects of the coordinated output power control should be considered, such as the SoC and ESS capacities. The unit with the highest SoC should supply more power to the common load to ensure a balanced discharge rate [8]. This coordinated control can be integrated into a hierarchical structure [9]. Several coordinated control strategies for SoC balance in a MG have been proposed [10]-[17] for centralized or distributed topologies by means of combining communication technology with hierarchical control. In [12] an adaptive virtual resistance (VR)-based droop controller is proposed to achieve stored energy balance. However, a centralized control is used, which needs point-to-point information exchanges, thereby increasing the communication network complexity and threatening the communication reliability because of a single point of failure (SPOF) issue. The SPOF causes the invalidation of entire high-level control.

Alternatively, distributed control methods have received

Yajuan Guan, Lexuan Meng , Chendan Li, Juan C. Vasquez, and Josep M. Guerrero are with Department of Energy Technology, Aalborg University, 9220 Aalborg, Denmark (e-mail: ygu@et.aau.dk, lme@et.aau.dk, che@et.aau.dk, juq@et.aau.dk, joz@et.aau.dk).

significant attention in MG control studies, because it offers a more robust system and guarantees uninterruptible operation when the network structure or the electrical parameters are changed. Therefore, it can effectively avoid SPOF and improve the reliability of the MG. A communication algorithm is required to guarantee a proper operation and prevent communication jam. Dynamic consensus algorithm (DCA) is one of the most promising distributed communication algorithms. DCA has been recently applied to MGs because information among DGs is effectively shared to facilitate the distributed coordination control [18]-[21]. When consensus algorithms are used, the communication links are only needed between neighboring DG units, which can achieve the plug 'n' play performance and reduce the communication cost. A distributed multi-agent-based algorithm is proposed in [15] to achieve SoC balance by voltage scheduling. A decentralized strategy based on fuzzy logic is proposed in [17] to ensure the stored energy balance for a DC MG by modifying VRs of droop controllers.

However, the aforementioned control strategies were all developed for implementation in DC MGs. Furthermore, most of these methods rely on droop control, which has a relatively slow transient response in the AC MGs caused by the average active and reactive power calculation when low-pass filters are used as shown in [22]. Moreover, the adaptive droop coefficients and variable voltage references seriously affect the system stability in droop-controlled systems [23], [24].

Additionally, stability analysis for consensus algorithm-based MG has not been sufficiently studied; the said MG includes an electrical part in the continuous-time domain and a consensus algorithm in the discrete-time domain. Modeling both parts in the discrete time domain is necessary to consider the discrete nature of communication. A generalized modeling method in the *z*-domain is proposed in [25], but the details are not given.

In this paper, a novel coordinated secondary control for balanced discharge rate of ESSs in an islanded AC MG is proposed. A DCA is implemented in each DG to share information for coordinately regulating the output power of DGs according to their SoC and ESS capacities by adjusting VRs of the paralleled voltage-controlled inverters (VCIs). Instead of modified droop control, an autonomous current-sharing controller is employed at the primary level for AC MG to achieve faster response and better accuracy relative to the control performance of droop control [26]. In addition, this control method provides a large stability margin during parameter variations [23]. To analyze the system stability and parameter sensitivity, a detailed discrete state-space model for *n*-node network in the *z*-domain is proposed; this model includes an electrical component, primary control, and DCA.

The paper is organized as follows. Section II introduces the islanded AC MG configuration. Section III introduces the proposed balanced discharge rate control. Section IV illustrates the detailed state-space model and stability analysis. Section V presents simulation and experimental results. Section VI concludes the paper.

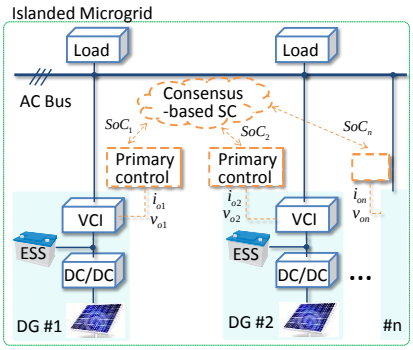

Fig. 1. PV-ESS-based AC MG case study scenario.

II. Islanded AC Microgrid Configuration

A photovoltaic (PV)-ESS-based islanded AC MG case-study scenario is shown in Fig. 1. The MG consists of several DG units, local loads, ESSs, power electronics interfaces, and secondary control (SC) loops. Each DG unit includes a DC/DC converter and a three-phase VCI, which is connected to the AC bus and powered by PV panels and ESSs. With the DCA-based distributed secondary control, the SoC coordination control is implemented in each DG unit.

According to the PV generation and load consumption, ESS can operate in charging or discharging modes during daylight. The main responsibility of the ESS during the day is to operate as a grid-forming unit and to balance the power between the PV panels and local loads.

At night, the ESS is still the grid-forming unit. The main role of the ESS at night is to establish the voltage magnitude and frequency, to feed local loads, and to provide the peak-shaving function caused by the lack of solar energy. In this scenario, only the ESSs are involved in the stability and reliability of the islanded MG. To prevent operation failure of MGs, the output power of the DG units should be coordinated to share the load according to their SoC and ESS capacities.

III. Proposed Balanced Discharge Rate Control

A. Primary control for current and power sharing

The autonomous current-sharing control strategy at the primary level is depicted in Fig. 2. The controller includes a synchronous-reference-frame phase-locked loop (SRF-PLL), a VR loop, and the proportional resonant inner voltage and current controllers [26]. Given this controller, the *d*-axis output current to angular frequency (I_{oq}–ω) and a *q*-axis output current to voltage magnitude (I_{od}–V) droop characteristics can be endowed in each inverter instead of adopting a conventional power droop control in an AC MG. The relationships of I_{od}, I_{oq}, R_{vird}, and R_{virq} can be expressed for N number of converters as:

$$I_{od1}R_{vird1} = I_{od2}R_{vird2} = \cdots = I_{odN}R_{virdN} \quad (1a)$$

$$I_{oq1}R_{virq1} = I_{oq2}R_{virq2} = \cdots = I_{oqN}R_{virqN} \quad (1b)$$

where R_{virdn} and R_{virqn} are the *d* and *q*-axis VRs of VCI #n.

Therefore, the *d*- and *q*-axis output currents can be independently regulated by adjusting the VRs based on different power rates or commands from higher level controllers. Additionally, the active and reactive power output sharing among the paralleled VCIs can be achieved from (1) by

This article has been accepted for publication in a future issue of this journal, but has not been fully edited. Content may change prior to final publication. Citation information: DOI 10.1109/TSG.2017.2672882, IEEE Transactions on Smart Grid

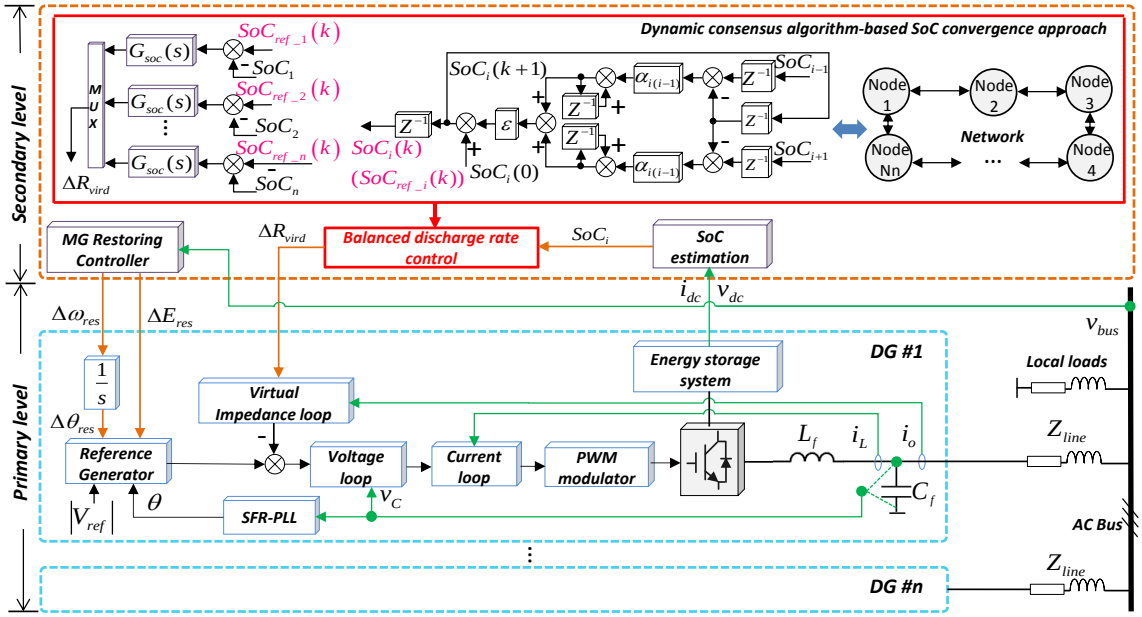

Fig. 2. Proposed DCA-based SoC coordinated control strategy.

multiplying the reference voltage. The active and reactive power outputs can be properly shared based on VR ratios as:

$$P_{o1}R_{virq1} = P_{o2}R_{virq2} = \ldots = P_{oN}R_{virqN} \quad (2a)$$

$$Q_{o1}R_{virq1} = Q_{o2}R_{virq2} = \ldots = Q_{oN}R_{virqN} \quad (2b)$$

where P_{on} and Q_{on} are the active and reactive power outputs.

B. SoC estimation and discharge rate calculation

The energy consumption of ESS$_i$ can be represented by the integration of the output active power of DG #i (P_i). Therefore, the SoC of ESS$_i$ can be calculated as:

$$SoC_i = 1 - {}^{k}\!/_{C_{bat\_i}} \int P_i \mathrm{d}t \quad (3)$$

where k is a time scale change ratio, which is equal to 1/3600; C_{bat_i} is the rated capacity of ESS$_i$; P_i is the active power output.

The discharge rate of DG #i (η_i) can be defined as:

$$\eta_i = \frac{d}{dt} SoC_i = -\frac{k}{C_{bat\_i}} P_i \quad (4)$$

The definition shows that the discharge rate is influenced by the rated capacity of ESS$_i$ and the active power output of DG #i. Thus, the coordinated control and the equal discharge rate can be obtained by regulating each VR based on their respective SoC and ESS capacities because the load sharing ratio among DG units is dominated by the VR ratio.

C. Information sharing with DCA

In a centralized control system, the reliability is highly dependent on the master DG unit. As the number of DGs increases, an increasing number of data also need to be exchanged, which may result in a communication jam. Furthermore, SPOF probably occurs to cause the invalidation of whole high-level control functions. To reduce the communication burden, to eliminate the dependence on a signal DG unit and therefore to improve the reliability and flexibility of an MG, a DCA-based SoC convergence approach is proposed in this paper. A DCA enables a set of distributed agents to agree on a control variable by exchanging information through communication networks and by facilitating the coordinated control among a large number of distributed agents. In this technique, each DG unit only communicates its state to adjacent DGs, thereby effectively reducing communication cost. Every DG in the network updates its state by providing a linear equation of its own state and neighbors' states. Finally, the states of all DGs can converge to the desired average value.

A connected MG system can be represented by a graph, $G_{MG} = (N_n, E)$, which is composed of a set of nodes, N_n, and a set of edges, E, as shown in Fig. 2. In this case, a node represents a DG unit. If i and j denote two different nodes, the edge, $\{i, j\} \in E$, presents a bidirectional communication link.

To maintain the accurate convergence in dynamically changing networks while handling the discrete communication data exchange, a DCA is applied as [20], [21]:

$$x_i(k+1) = z_i + \varepsilon \sum_{j \in N_i} \delta_{ij}(k+1) \quad (5a)$$

$$\delta_{ij}(k+1) = \delta_{ij}(k) + \alpha_{ij}\left(x_j(k) - x_i(k)\right) \quad (5b)$$

being $\bar{x} = \frac{1}{N}\sum_{i=1}^{N} z_i$,

where x_i and x_j are the states stored in nodes i and j; $i, j = 1, 2, \ldots, N$, $\{i, j\} \in E$; α_{ij} represents the connection status between nodes i and j; ε is the constant edge weight; $\delta_{ij}(0)$ is equal to zero. Thus, the final convergence value is related to the initial state, z_i, which indicates that regardless of the degree of change that occurs in z_i, the algorithm can converge to the desired average value.

Regarding the real physical meaning, the output variables, $x_i(k+1)$, $i, j = 1, 2, \ldots, N$, and $\{i, j\} \in E$, become the SoC references, SoC_{ref_i}, for each DG unit in this paper. Thus, (5) can be rewritten as:

$$SoC_{ref\_i}(k+1) = SoC_i + \varepsilon \sum_{j \in N_i} \delta_{ij}(k+1) \quad (6a)$$

$$\delta_{ij}(k+1) = \delta_{ij}(k) + \alpha_{ij}\left(SoC_j(k) - SoC_i(k)\right) \quad (6b)$$

The edge weight constant, ε, affect the convergence stability

and dynamic. The range of ε over which convergence is obtained can be determined as [27]:

$$0 < \varepsilon < \frac{2}{\lambda_1(\boldsymbol{L})} \tag{7}$$

where $\boldsymbol{L}$ is the Laplacian matrix of graph G_{MG} that is defined as $\boldsymbol{L} = \boldsymbol{A}\boldsymbol{A}^{\mathrm{T}}$ [28], and

$$\boldsymbol{A}_{ij} = \begin{cases} 1 & \textit{if edge } l \textit{ starts from node } i, \\ -1 & \textit{if edge } l \textit{ ends at node } i, \\ 0 & \textit{otherwise.} \end{cases},$$

$\lambda_1(\boldsymbol{L})$ is the largest eigenvalue of $\boldsymbol{L}$.

Therefore, as long as edge weight constant ε is between zero and $2/\lambda_1(\boldsymbol{L})$, the convergence can be guaranteed.

Furthermore, ε can be taken as a turning parameter to minimize the convergence time for a given communication network when it meets the following equation [27]:

$$\varepsilon = \frac{2}{\lambda_1(\boldsymbol{L}) + \lambda_{n-1}(\boldsymbol{L})} \tag{8}$$

where $\lambda_{n-1}(\boldsymbol{L})$ denotes the second smallest eigenvalue of the $\boldsymbol{L}$.

If a ten-node network with ring connection and bidirectional communication links is considered, the eigenvalues of $\boldsymbol{L}$ are $[0\ 0.382\ 0.382\ 1.382\ 1.382\ 2.618\ 2.618\ 3.618\ 3.618\ 4]^{\mathrm{T}}$. Thereby, the convergence condition range calculated by (7) is $0 < \varepsilon < 0.5$, and the optimal edge weight constant ε is equal to 0.23.

D. Proposed coordinated secondary control for balanced discharge rate

The complete control scheme of the proposed DCA-based SoC coordinated secondary control strategy is shown in Fig. 2. At the secondary control level, DCA is implemented for convergence by information exchange. In this case, the DCA finds the averaged value of SoC for each DG based on the outputs of SoC estimation loops and the network configuration. $\Delta\omega_{res}$ and ΔE_{res} are used for angular frequency and voltage magnitude restoration. Hypothetically, each ESS is fully charged at the beginning, which means that each initial SoC is equal to 1. The discharge rate of each DG unit should be balanced according to its ESS capacities to avoid overcurrent and unintentional outage. The difference between the measured SoC_i and the desired average SoC_{ref_i} obtained from DCA is sent to a PI controller, the output of which is presented as an increment in the *d*-axis VR to adjust the output current of DG #*i*. The increment of the *d*-axis VR can be expressed as:

$$\Delta R_{vird\_i} = K_p(SoC_{ref\_i} - SoC_i) + K_i\int(SoC_{ref\_i} - SoC_i)dt \tag{9}$$

where K_p and K_i are the parameters of the PI controllers. To reduce the power oscillation, the outputs of PI controllers are regarded as incremental control parts. Therefore, the updated *d*-axis VR of DG #*i* can be presented as:

$$R_{vird\_i} = R_{vird\_b} + \Delta R_{vird\_i} \qquad i = 1,2,3,4.....N \tag{10}$$

where R_{vird_i} is the *d*-axis VR for DG #*i*; R_{vird_b} is the basic *d*-axis VR; in this case, R_{vird_b} is preassigned to 4 Ω [26]; ΔR_{vird_i} is the increment outputs from the PI controller.

Therefore, the adaptive *d*-axis VRs can be considered as turning parameters to adjust the direct current outputs and active power outputs of parallel-connected DG units with respect to their SoC values and different ESS capacities.

IV. State-space Model and Stability Analysis

To analyze the system stability and parameter sensitivity for a large network with numerous nodes, the developed state-space model for the proposed coordinated secondary controller-based *n*-node network is discussed in this section. The detailed structure of the state-space models is depicted by the block diagram in Fig. 3(a). The small-signal state-space model is mainly divided into two parts: the green block is in the continuous time domain whereas the orange block is in the discrete time domain.

A. SoC *controller*

The model of SoC estimation loop can be derived as:

$$[\hat{X}_1] = A_{X1}[X_1] + B_{X1}[P] \tag{11}$$

being $X_1 = \left[X_{1\_1}\ X_{1\_2}\cdots X_{1\_N}\right]^T$, $P = \left[P_1\ P_2\cdots P_N\right]^T$,

$A_{X1} = [0]_{(N\times N)}$, $B_{X1} = I_{(N\times N)}$,

where $\hat{}$ denotes the derivative with respect to time; X_{1_i} represents the state variable X_1 of DG #*i* (*i*=1, 2, … , *N*); P_i is the active power output of DG #*i*; *I* is identity matrix.

The difference between SoC_i and the SoC reference, SoC_{ref_i}, input into a PI controller whose output is taken as an increment in VR to adjust the output current of DG #*i*.

The variables of the PI controller and low-pass filter can be expressed as:

$$[\hat{X}_2] = A^1_{X2}[X_1] + A^2_{X2}[X_2] + A^3_{X2}[X_3] + B^1_{X2}\left[SoC_{ref}\right] + B^2_{X2}[1]_{(N\times 1)} \tag{12}$$

being $X_2 = \left[X_{2\_1}\ X_{2\_2}\cdots X_{2\_N}\right]^T$, $X_3 = \left[X_{3\_1}\ X_{3\_2}\cdots X_{3\_N}\right]^T$,

$SoC_{ref} = \left[SoC_{ref\_1}\ SoC_{ref\_2}\cdots SoC_{ref\_N}\right]^T$, $A^2_{X2} = A^3_{X2} = [0]_{(N\times N)}$,

$A^1_{X2} = diag\left(\frac{k}{C_{bat\_1}}, \frac{k}{C_{bat\_2}}, \cdots, \frac{k}{C_{bat\_N}}\right)$, $B^1_{X2} = I_{(N\times N)}$, $B^2_{X2} = -I_{(N\times N)}$,

where X_{2_i} represents the state variable X_2 of DG #*i*; SoC_{ref_i} denotes the SoC reference value for DG #*i*.

$$[\hat{X}_3] = A^1_{X3}[X_1] + A^2_{X3}[X_2] + A^3_{X3}[X_3] + B^1_{X3}\left[SoC_{ref}\right] + B^2_{X3}[1]_{(N\times 1)} \tag{13}$$

being $A^1_{X3} = diag\left(\frac{kK_p\omega_c}{C_{bat\_1}}, \frac{kK_p\omega_c}{C_{bat\_2}}, \cdots, \frac{kK_p\omega_c}{C_{bat\_N}}\right)$, $A^2_{X3} = K_i\omega_c[I]_{(N\times N)}$,

$A^3_{X3} = -\omega_c[I]_{(N\times N)}$, $B^1_{X3} = K_p\omega_c[I]_{(N\times N)}$,

$B^2_{X3} = \left(R_{vird\_b} - K_p\right)\omega_c[I]_{(N\times N)}$,

where X_{3_i} represents the state variables X_3 of DG #*i*; K_p and K_i denote the proportional and integral coefficients; ω_c is equal to $1/\tau$, which is the cutoff frequency of the inertia unit.

B. MG plant

If the three DG units are connected in a parallel manner to feed the total load consumption (P_{load}), the active power output of DG #*i* is determined by VR ratios, as shown in Fig. 3 (a). The active power output of DG #*i* can be described as:

$$P_i = \frac{1/X_{3\_i}}{1/X_{3\_1} + 1/X_{3\_i} + \cdots + 1/X_{3\_N}} P_{load} \tag{14}$$

The power balance between the generated power of DGs and the load power are related to two aspects. The first is that owing

This article has been accepted for publication in a future issue of this journal, but has not been fully edited. Content may change prior to final publication. Citation information: DOI 10.1109/TSG.2017.2672882, IEEE Transactions on Smart Grid

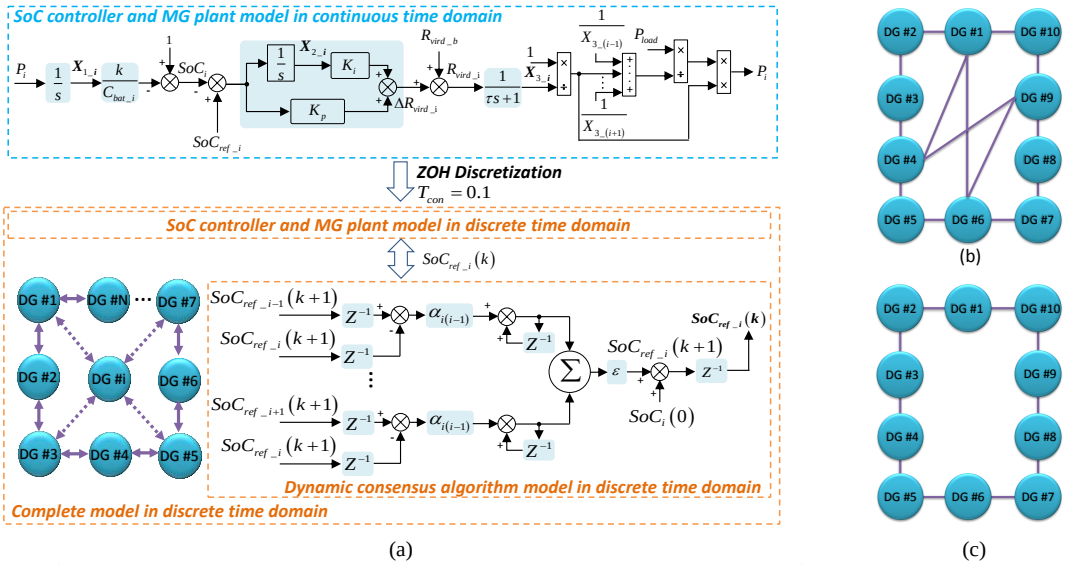

Fig. 3. Block diagram of the small-signal state-space model and communication topology. (a) Block diagram of the model. (b) Cross shape. (c) Ring shape.

to the presence of ESSs, the DC bus voltage can be regarded as a constant value during islanded operation. Therefore, in steady state, the total active power output of the DGs is equal to the load power when only resistive load is included in the system. The second aspect is that when the load changes, the total generated power changes accordingly. This change is decided by the inherent I_{od}-V, I_{oq}-ω droop characteristics [26]. After a transient period, the generated power of DGs increases to fulfill the load requirements. The power sharing among the parallel DGs is proportional to the VR ratio. Since (14) presents the relationship between the total active power output of the DGs and the total load power, they should be equal in steady state.

The real-valued function, P_i, is differentiable at the equilibrium point; thus, a linear approximation of P_i is determined by Taylor's formula at this point:

$$P_i = P_i^{equ} + \sum_{k=1}^{N}\left[a_{n\_k}(X_{3\_k} - X_{3\_k}^{equ})\right] \tag{15}$$

being $a_n = \left[a_{n\_1}\ a_{n\_2}\cdots a_{n\_N}\right]_{1\times N}$,

$$a_{n\_k(k\neq n)} = \frac{P_{load}\prod_{i=1..N,i\neq 1,i\neq n} x_{3\_i}^{equ}}{\sum_{j=1}^{N}\prod_{i=1..N,i\neq j} x_{3\_i,\,j}^{equ}} - \frac{P_{load}\left(\prod_{i=1..N,i\neq n} x_{3\_i}^{equ}\right)\left(\sum_{i=1,i\neq 1}^{N} x_{3\_i}^{equ}\right)}{\left(\sum_{j=1}^{N}\prod_{i=1..N,i\neq j} x_{3\_i,\,j}^{equ}\right)^2},$$

$$a_{n\_n} = \frac{-P_{load}\left(\prod_{i=1..N,i\neq n} x_{3\_i}^{equ}\right)\left(\sum_{i=1,i\neq n}^{N} x_{3\_i}^{equ}\right)}{\left(\sum_{j=1}^{N}\prod_{i=1..N,i\neq j} x_{3\_i,\,j}^{equ}\right)^2}$$

where the state variables with *equ* as the superscript are the steady-state values at equilibrium point.

Therefore, the state variables X_{1_i} in (11) can be updated in terms of the relationship between the output power and the state variables X_{1_i}, X_{2_i}, and X_{3_i}:

$$\left[\hat{X}_1\right] = A_{X1}^1\left[X_1\right] + A_{X1}^2\left[X_2\right] + A_{X1}^3\left[X_3\right] + B_{X1}^1\left[X_3^{equ}\right] + B_{X1}^2\left[P^{equ}\right] \tag{16}$$

being $X_3^{equ} = \left[X_{3\_1}^{equ}\ X_{3\_2}^{equ}\cdots X_{3\_N}^{equ}\right]^T$, $P^{equ} = \left[P_1^{equ}\ P_2^{equ}\cdots P_N^{equ}\right]^T$,

$A_{X1}^1 = [0]_{(N\times N)}$, $A_{X1}^2 = [0]_{(N\times N)}$, $A_{X1}^3 = [a_1\ a_2\cdots a_N]_{N\times N}^T$,

$B_{X1}^1 = [-a_1\ -a_2\cdots -a_N]_{N\times N}^T$, $B_{X1}^2 = [I]_{(N\times N)}$,

C. Combination of SoC controller and MG plant models

The overall state-space models of the SoC controller and MG plant in the continuous time domain can be derived by integrating the state-space models of X_{1_i}, X_{2_i}, and X_{3_i} as:

$$\left[\hat{X}_c^{con}\right] = A_c^{con}\left[X_c^{con}\right] + B_c^{1\_con}\left[u_c^{1\_con}\right] + B_c^{2\_con}\left[u_c^{2\_con}\right] \tag{17}$$

being $\left[u_c^{1\_con}\right] = \left[SoC_{ref\_1}\ SoC_{ref\_2}\cdots SoC_{ref\_N}\right]^T$,

$\left[u_c^{2\_con}\right] = \left[X_{3\_1}^{equ}\ X_{3\_2}^{equ}\cdots X_{3\_N}^{equ}\ P_1^{equ}\ P_2^{equ}\cdots P_N^{equ}\ 11\cdots 1\right]_{(1\times 3N)}^T$,

$\left[X_c^{con}\right] = \left[X_{1\_1}\cdots X_{1\_N}\ X_{2\_1}\cdots X_{2\_N}\ X_{3\_1}\cdots X_{3\_N}\right]_{(3N\times 1)}^T$,

$$A_c^{con} = \begin{bmatrix} A_{X1}^1 & A_{X1}^2 & A_{X1}^3 \\ A_{X2}^1 & A_{X2}^2 & A_{X2}^3 \\ A_{X3}^1 & A_{X3}^2 & A_{X3}^3 \end{bmatrix},\ B_c^{1\_con} = \begin{bmatrix} 0_{(N\times N)} \\ B_{X2}^1 \\ \vdots \\ B_{X3}^1 \end{bmatrix},\ B_c^{2\_con} = \begin{bmatrix} B_{X1}^1 & B_{X1}^2 & 0_{(N\times N)} \\ 0_{(N\times N)} & 0_{(N\times N)} & B_{X2}^2 \\ 0_{(N\times N)} & 0_{(N\times N)} & B_{X3}^2 \end{bmatrix}$$

In the integrated overall state-space model for the SoC controller and MG plant, SoC_{ref_i} are input signals that are actually the output from the *SoC* DCA loop. Given that DCA is in a discrete time domain, which has a fixed sampling time (T_{con}), the combined model of the SoC controller and MG plant needs to be discretized for integration with the DCA model. The zero-order-hold (ZOH) method with the same sampling time of T_{con} is applied for discretized transformation.

The discrete time form of (17) can be expressed as:

$$X_c^{dis}(k+1) = G_c^{dis}X_c^{dis}(k) + H_c^{1\_dis}u_c^{1\_dis}(k) + H_c^{2\_dis}u_c^{2\_dis}(k) \tag{18}$$

being $G_c^{dis} = e^{A_c^{con}T_{con}}$, $H_c^{1\_dis} = \left(\int_0^{T_{con}} e^{A_c^{con}\sigma}d\sigma\right)B_c^{1\_con}$,

$H_c^{2\_dis} = \left(\int_0^{T_{con}} e^{A_c^{con}\sigma}d\sigma\right)B_c^{2\_con}$

D. DCA

As shown in Fig. 3 (a), the inputs of the SoC DCA loop are

This article has been accepted for publication in a future issue of this journal, but has not been fully edited. Content may change prior to final publication. Citation information: DOI 10.1109/TSG.2017.2672882, IEEE Transactions on Smart Grid

the initial SoC states of DG units, whereas the outputs are the states obtained for each DG at the *k*th iteration, $SoC_{ref\_i}(k)$. Based on (5a) and (5b), two state variables exist in the DCA control loop. One of the state variables is the internal cumulative difference between nodes *i* and *j*, $\delta_{ij}(k)$, with $j \in N_i$ which is the set of neighbors of node *i*. The other variable is the output state $x_i(k)$, which has a practical physical meaning of $SoC_{ref\_i}(k)$. The state-space model of DCA can be described as:

$$X_{con}^{dis}(k+1) = G_{con}^{dis} X_{con}^{dis}(k) + H_{con}^{dis} u_{con}^{dis} \tag{19}$$

being $u_{con}^{dis} = \left[SoC_{ref\_1}(0) \;\; SoC_{ref\_2}(0) \cdots SoC_{ref\_N}(0) \right]^T_{(1\times N)}$

$$X_{con}^{dis} = \left[\delta_{12} \cdots \delta_{1N} \cdots \delta_{N1} \cdots \delta_{N(N-1)} \; SoC_{ref\_1} \cdots SoC_{ref\_N} \right]^T_{\left(1\times N^2\right)},$$

$$G_{con}^{dis} = \begin{bmatrix} G_{con\_11}^{dis} & G_{con\_12}^{dis} \\ G_{con\_21}^{dis} & G_{con\_22}^{dis} \end{bmatrix}_{\left(N^2\times N^2\right)}, G_{con\_11}^{dis} = I_{\left(\left(N^2-N\right)\times\left(N^2-N\right)\right)},$$

$$G_{con\_12}^{dis} = \begin{bmatrix} -\alpha_{12} & \alpha_{12} & & 0_{1(N-2)} \\ & \vdots & & \\ -\alpha_{1N} & 0_{1(N-2)} & & \alpha_{1N} \\ \alpha_{21} & -\alpha_{21} & & 0_{1(N-2)} \\ & \vdots & & \\ 0 & -\alpha_{2N} & 0_{1(N-3)} & \alpha_{2N} \\ \alpha_{N1} & 0_{1(N-2)} & & -\alpha_{N1} \\ & \vdots & & \\ 0_{1(N-2)} & \alpha_{(N-1)N} & & -\alpha_{(N-1)N} \end{bmatrix}_{\left(\left(N^2-N\right)\times N\right)},$$

$$G_{con\_21}^{dis} = \begin{bmatrix} [\varepsilon]_{(1\times(N-1))} & 0 & 0 & 0 \\ 0 & [\varepsilon]_{(2\times(N-1))} & 0 & 0 \\ 0 & 0 & \ddots & 0 \\ 0 & 0 & 0 & [\varepsilon]_{(N\times(N-1))} \end{bmatrix}_{\left(N\times\left(N^2-N\right)\right)},$$

$$G_{con\_22}^{dis} = \begin{bmatrix} -\varepsilon\sum_{i=1,i\neq1}^{N}\alpha_{1i} & \varepsilon\alpha_{12}\cdots & \varepsilon\alpha_{1N} \\ \varepsilon\alpha_{21} & -\varepsilon\sum_{i=1,i\neq2}^{N}\alpha_{1i}\cdots & \varepsilon\alpha_{2N} \\ & \ddots & \\ \varepsilon\alpha_{21} & \varepsilon\alpha_{21}\cdots & -\varepsilon\sum_{i=1,i\neq N}^{N}\alpha_{Ni} \end{bmatrix}_{(N\times N)},$$

$$H_{con}^{dis} = \begin{bmatrix} H_{con\_11}^{dis} \\ H_{con\_21}^{dis} \end{bmatrix}_{\left[N^2\times N\right]}, \; H_{con\_11}^{dis} = [0]_{\left(\left(N^2-N\right)\times N\right)}, \; H_{con\_21}^{dis} = I_{(N\times N)}$$

E. Combined model of the system

Based on (11)-(19), a complete linearized discrete state-space model of the proposed *n*-node network can be obtained by combining the following sub-state-space models: the combined SoC controller and MG plant model in the discrete time domain and the DCA model. A total of N^2+3N states are included:

$$X^{dis}(k+1) = G^{dis} X^{dis}(k) + H^{dis} u^{dis} \tag{20}$$

being $X^{dis} = [X_{1\_1}\cdots X_{1\_N} \; X_{2\_1}\cdots X_{2\_N} \; X_{3\_1}\cdots X_{3\_N} \; \delta_{12}\cdots\delta_{1N} \cdots\delta_{N1}\cdots\delta_{N(N-1)} \; SoC_{ref\_1}\cdots SoC_{ref\_N}]^T_{\left(1\times\left(N^2+3N\right)\right)}$

$$u^{dis} = \left[u_c^{2\_dis} \;\; u_{con}^{dis} \right]^T_{((3N+N)\times1)},$$

$$G^{dis} = \begin{bmatrix} G_c^{dis} & \left[0_{\left(3N\times\left(N^2-N\right)\right)} \;\; H_c^{1\_dis} \right] \\ 0_{\left(N^2\times3N\right)} & G_{con}^{dis} \end{bmatrix}, \; H^{dis} = \begin{bmatrix} H_c^{2\_dis} & 0_{(3N\times N)} \\ 0_{\left(N^2\times3N\right)} & H_{con}^{dis} \end{bmatrix}$$

In this model, the number of DG units can be changed by adjusting *N*. Meanwhile, a change in matrix G_{con}^{dis} will change the communication topology. Thus, the developed *n*-DG state-space model can exhibit an arbitrary number of DG units with random communication topologies.

F. Convergence condition and communication topology

In order to maintain stable operation in a large network with numerous participants, two aspects have to be confirmed. The first aspect is that, generally, fast communication is expected to provide fast convergence. However, in this case, low-bandwidth communication is better, e.g., information exchanges every 100 ms to avoid undesirable interaction between different control levels. The bandwidth of inner voltage and current loops are normally designed at 1/5-1/10 of switching frequency (10 kHz). Besides, secondary control should be 6 times slower than the primary control as explained in [29]. Therefore, the communication links with 100 ms time step fulfill the requirements. The major issue that may affect the system stability is the communication fault of the secondary control. Some previous studies [29], [30] investigated the effect of communication latency on the secondary control in MGs. In [29], both centralized and decentralized controllers present good performance for a time delay of 200 ms. However, the centralized controller does not work effectively when communication delay is up to 1 s. By contrast, the decentralized control strategy is stable with a delay of 4 s. Second, as mentioned above, the edge weight constant ε should between zero and $2/\lambda_1(L)$ to ensure the stable convergence.

Communication topology of a network is usually decided by nodes' geographical distribution. Nearby nodes are preferentially connected. Therefore, in a certain network, the analysis of consensus problems reduces to spectral analysis of Laplacian based on the network topology. In order to guarantee system stability and fast convergence of communication algorithm, edge weight constant ε has to be properly chosen based on communication topology and the corresponding eigenvalues by using (7) and (8). The main idea is actually to minimize the spectral radius with certain constraints on the weight matrix. In addition, second smallest eigenvalue of Laplacian matrix λ_{n-1} is named algebraic connectivity of the graph. λ_{n-1} is a measure of convergence speed of the consensus algorithm [31]. A network with a relatively high algebraic connectivity is necessarily robust to both node-failures and edge-failures. Fast convergence speed of consensus algorithm can help to ensure stable operation of electrical parts.

In case of a variable communication network, topologies seriously influence the network dynamics [25]. The fastest convergence speed can be obtained with fully-connected network. However it obviously increases the communication

This article has been accepted for publication in a future issue of this journal, but has not been fully edited. Content may change prior to final publication. Citation information: DOI 10.1109/TSG.2017.2672882, IEEE Transactions on Smart Grid

cost. Ring shape is an acceptable choice by considering the tradeoff between communication cost and convergence performance. Given all that, a better communication topology of a network can be obtained by considering geographical distribution, convergence condition calculation, improved algebraic connectivity, fastest edge weight constant and communication cost.

G. SoC PI controller design

Each connected DG unit uses the same SoC PI controller. In order to design the parameters for this PI controller, a general study case should be considered. In this case, DG #*i* has a SoC disturbance, and the rest of the DG units operate with basic VR. According to (14) and Fig. 3(a), the small-signal closed loop transfer function T (s) can be described as follows:

$$T(s)=\frac{\Delta P_i}{\Delta SoC_{ref\_i}}=\frac{K_p\omega_c K_T C_{bat\_i}s+K_i\omega_c K_T C_{bat\_i}}{C_{bat\_i}s^3+\omega_c C_{bat\_i}s^2-K_p\omega_c K_T ks-K_i\omega_c K_T k} \quad (21)$$

being $K_T=\dfrac{-R_{vird\_b}P_{load}(N-1)}{\left[R_{vird\_b}+(N-1)X_{3\_i}\right]^2}$,

where N is equal to the number of DG units; in this case, N=10.

To obtain the desired control performance, some specifications need to be indicated, e.g., settling time and damping ratio. In this study, the damping ratio is set to 0.7, and the settling time is around 70 ms. Hence, the designed K_p and K_i are equal to 12 and 1000, respectively.

H. Stability analysis based on linearized discrete model

To analyze the system stability and adjust the parameters for obtaining the desired transient response of the proposed system, *z*-domain root locus plots of (20) are represented as functions of different parameter variations. A ten-node network with two topologies is considered. The first topology is cross shaped as shown in Fig. 3(b). The second topology is ring shaped, which is the most common topology with the consensus algorithm, as shown in Fig. 3(c). The system parameters and equilibrium point are listed in Table I.

Fig. 4 shows the root locus in the discrete-time domain for the system with the cross topology as a function of the variation of the proportional term in the SoC regulator, K_p, from 1 to 2000. The system has a damped response for higher values of K_p. The system could maintain its stability as the eigenvalues are displaced within the unit circle. If K_p continuously increases, the system will become unstable.

Fig. 5 shows the root locus plot for the system with a cross topology that corresponds to a variation of the integral term, K_i, from 100 to 5000. The figure shows that an increase in K_i leads to complex conjugated dominating poles, which induce oscillations.

TABLE I
MODEL PARAMETERS AND EQUILIBRIUM POINT

Model Parameters										
$C_{bat\_1/2/3\_e}$	10/20/30 Wh						K_p	12		
$C_{bat\_1\cdots10\_s}$	20/22/24/26/28/30/32/34/36/38 Wh									
$R_{vird\_b1\cdots10}$	4 Ω			K_i	1000		k	1/3600		
Equilibrium Point										
$R^{equ}_{vird\_1\cdots10}$	1.7	1.9	2.1	2.3	2.6	3	3.5	4.2	5.2	7
$SoC_{ref\_1\cdots10}(0)$	1	1	1	1	1	1	1	1	1	1

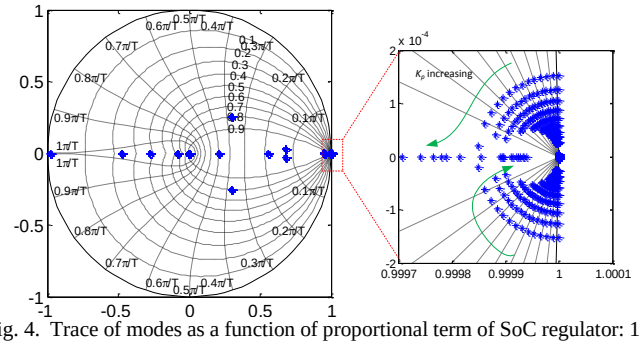

Fig. 4. Trace of modes as a function of proportional term of SoC regulator: 1 < K_p< 2000, (cross topology).

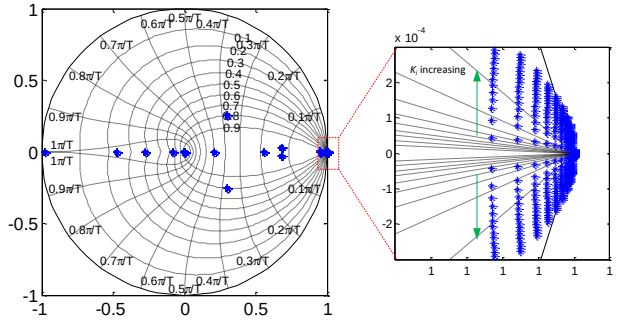

Fig. 5. Trace of modes as a function of integral term of SoC regulator: 100 < K_i < 5000, (cross topology).

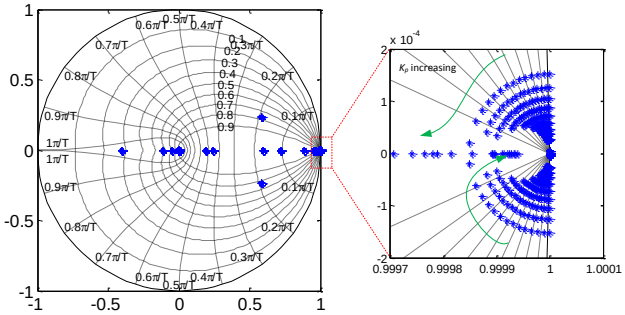

Fig. 6. Trace of modes as a function of proportional term of SoC regulator: 1 < K_p < 2000, (ring topology).

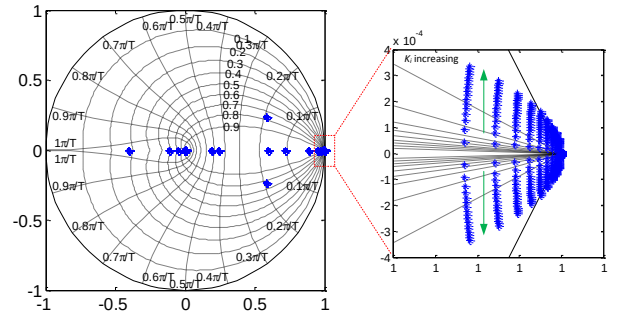

Fig. 7. Trace of modes as a function of integral term of SoC regulator: 100 < K_i < 5000, (ring topology).

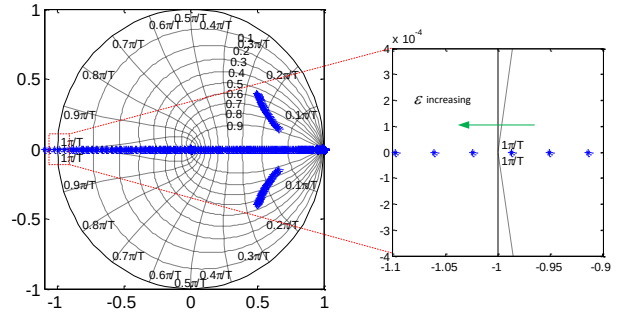

Fig. 8. Trace of modes as a function of edge weight constant of DCA: 0.2 < ε < 0.6, (ring topology).

Fig. 6 shows the root locus for the system with a ring topology when K_p in the SoC regulator changes from 1 to 2000. The system similarly presents a damped response for higher values of K_p.

Fig. 7 shows the root locus plot for the system with a ring topology that corresponds to a variation of K_i from 100 to 5000. Complex conjugated dominating poles appear as K_i increased.

The root locus plot for the ring-connected network with the varying of edge weight, ε from 0.2 to 0.6, is shown in Fig. 8. The upper limit of ε under the ring topology for maintaining the stable convergence is equal to 0.5. It can be seen from Fig. 8, as the value of ε increases, oscillation appears in the DCA dynamic. When ε is equal to 0.52, the poles cross the unit circle that indicates the stable convergence cannot be guaranteed.

As illustrated in Figs. 4 and 8, the paralleled DGs with the proposed controller present the low sensitivity of parameters at the secondary level over the system dynamics. This trend is attributed to the large stability margin provided by the employed autonomous current sharing control at the primary level [22]. Therefore, the proposed control approach can achieve more stable control performance compared with the droop-based SoC coordinated controller.

V. Simulation and Experimental Results

To verify the effectiveness of the proposed DCA-based coordinated control strategy in various case-study scenarios, simulations based on a ten-node network and experiments from a three-DG-unit system were conducted. The three-DG-unit islanded system consisted of three Danfoss 2.2 kW inverters, a real-time dSPACE1006 platform, *LC* filters, and resistive loads, as shown in Fig. 9. The Danfoss inverters were used to simulate different DG units with different ESS capacities. The electrical setup and control system parameters are listed in Table II. dSPACE 1006 provides the computing power for the real-time system and also functions as an interface to the I/O boards and the host PC. The control models in Matlab/Simulink can be programmed from Simulink to the DS1006 processor board of dSPACE real-time control platforms via real-time interface. The communication links and consensus algorithm in this paper were formulated in Simulink and dSPACE with the time step T_{con}=100 ms. For real applications, C, C++, and Python programming languages can be used for the communication network.

Before the simulations and experiments were conducted, the required assumptions were met. First, ESS_i in each DG unit was fully charged. Thus, each $SoC_{ref\_i}(0)$ was equal to 1. Second, the minimum threshold of SoC was set at 0.3. Third, the ESS capacities were different. C_{bat_1}, C_{bat_2}, and C_{bat_3} were equal to 10, 20, and 30 Wh in the experiments. In the simulations, the values of $C_{bat\_1/2/.../10}$ were from 20 to 38 Wh. Fourth, the maximum output power of each DG unit was assumed to be 1000 W.

A. Experimental results with conventional power-sharing control

The experimental results of SoC values, output powers, and SoC change rates for DGs that use the traditional power sharing control strategy are illustrated in Figs. 10(a)-(c), respectively. The figures show that the three DG units were initially operating on a parallel level, with equal output powers feeding approximately 209 W by means of the proposed primary control and the same VRs to supply R_{load1}. In this condition, their SoC values decreased at different rates because the rated capacities of the ESSs were different. At 50 s, an extra 230 Ω load (R_{load2}) was connected to the parallel-connected DG system, which caused a real power step change of approximated 209 W in each DG unit. With the unified output power, SoC_1 decreased the fastest because of the smallest ESS capacity of DG #1. At 87s, DG #1 was shut down as SoC_1 reached 0.3, as shown in Fig. 10(a). Meanwhile, the corresponding real power outputs of DGs #2 and #3 increased by 209 W to supply the needed load, which intensely decreased the SoC_2 and SoC_3, as shown in Figs.10(a) and (b). At 129 s, DG #2 was suddenly shut down as SoC_2 reached 0.3, leaving DG #3 to solely supply the total amount of needed power. As displayed in Fig. 10(b), the output power of DG #3 had to increase to around 1.2 kW, which is over the maximum output power of each DG (P_{max_3}). Obviously, a serious risk of operation failure exists because of the over current in real applications. In this condition, the rated capacities of all the DGs have to be increased by an allowance to avoid affecting MG reliability. Moreover, the faster the ESSs discharge in practice, the less total electrical energy can be obtained.

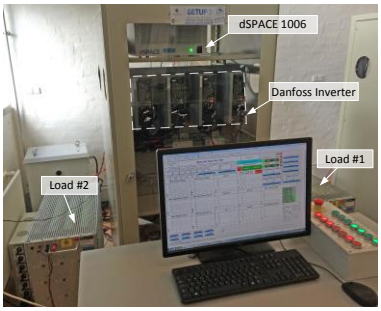

Fig. 9. Experimental setup.

TABLE II
Power Stage and Control System Parameters

Symbol	Description	Value
V_{dc}/ V_{MG}	DC voltage/ MG voltage	650/ 311 V
f/ f_s	MG frequency/ Switching frequency	50/ 10k Hz
$P_{max\_1/2/3}$	Maximum output power of DG 1/2/3	1 kW
L_f/ C_f	Filter inductance/ Filter capacitance	1.8 mH/ 25 µF
$R_{load1/2}$	Common load #1/ Common load #2	230/ 230 Ω
k_{pi}/ k_{ii}	Proportional/ Integral term in current controller	0.07/ 0
k_{pv}/ k_{iv}	Proportional/ Integral term in voltage controller	0.04/ 94
k_{p_PLL}/ k_{i_PLL}	PLL proportional/ integral term	1.4/ 1000

B. Experimental results with proposed DCA-based coordinated control strategy

The experimental results of SoC values, output powers, and SoC change rates for DGs with the proposed DCA-based coordinated control strategy are illustrated in Figs. 11(a)-(c), respectively. In this test, the VR of each DG unit was regulated based on the difference between the measured SoC and SoC reference output from the distributed DCA-based coordinated controller. The SoC reference outputs were related to different ESS capacities. As mentioned above, each DG unit only communicated its SoC state to adjacent DGs when obtaining a new SoC state via a linear equation. Finally, the adaptive VR ratio determined the power-sharing ratio among the connected

This article has been accepted for publication in a future issue of this journal, but has not been fully edited. Content may change prior to final publication. Citation information: DOI 10.1109/TSG.2017.2672882, IEEE Transactions on Smart Grid

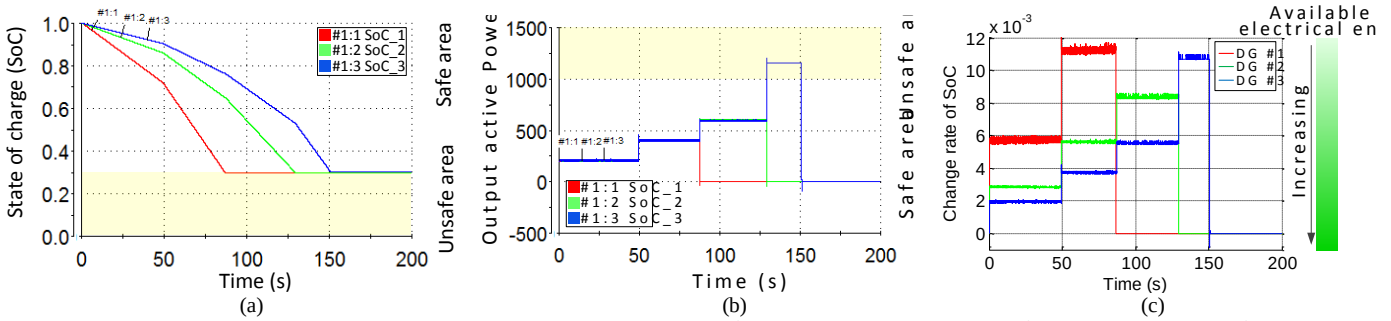

Fig. 10. Experimental results with the conventional power sharing control. (a) SoC of ESSs. (b) Active power output of DGs. (c) Change rates of SoC.

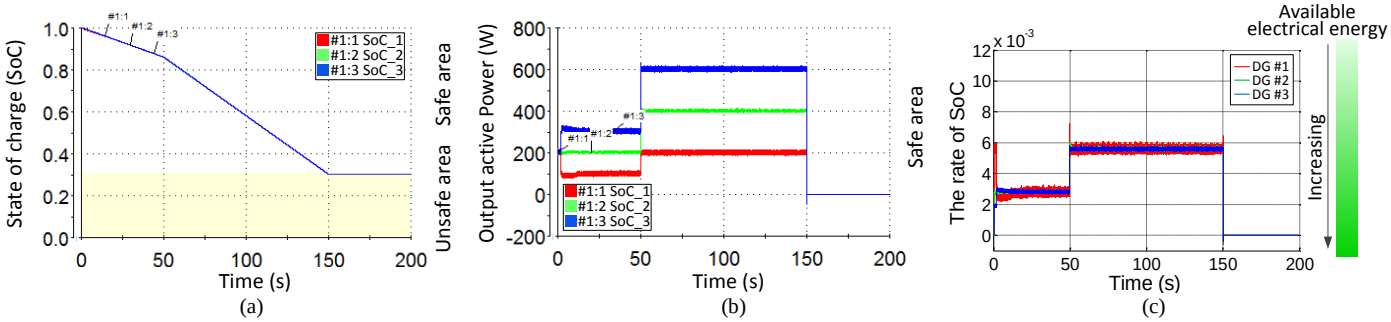

Fig. 11. Experimental results with the proposed DCA-based coordinated control. (a) SoC of ESSs. (b) Active power output of DGs. (c) Change rates of SoC.

DG units. Fig. 11(a) shows that, the three DG units were initially operating in a parallel manner without any coordinated control. After approximately 5 s, the proposed DCA-based coordinated secondary controller started to function. The SoC values decreased with the same gradient from the original. Given that the respective ESS capacities of these three DG units were pre-assigned at 10/20/30 Wh (a ratio of 1:2:3), the load-power sharing ratio among the parallel-connected DG units was also equal to 1:2:3. At 50 s, a load step-up change (R_{load2}) created power step changes among the paralleled DG units with an equal proportion of 1:2:3. At 150 s, SoC_1, SoC_2, and SoC_3 simultaneously decreased to 0.3. This control performance is guaranteed by the proposed coordinated secondary controller and the adaptive VRs at the primary level. Notably, overcurrent never appeared during this test, thereby implying that operation failure can be effectively prevented. Therefore, the reliability of the entire system can be improved. Additionally, the redundant capacities and costs of the DG units can be reduced. Moreover, the lower discharge rates of ESSs were achieved by the proposed method, as shown in Fig. 11(c), can help ESSs provide more electrical energy.

C. Comparison of experimental results with different control strategies during communication fault

The experimental results from the centralized average control and the proposed DCA-based coordinated control during an online excluding/including DG unit are shown in Figs. 12 and 13 for comparison.

As displayed in Fig. 12(b), at t_1, load #2 was connected to three paralleled DG units as a load step-up disturbance. At t_2, DG #1 was disconnected from the MG central controller (MGCC) in the case of communication fault or intentional operation, as shown in Fig. 12(a). Fig. 12(b) shows that, the parallel-connected DG system cannot proportionally share the load according to their ESS capacities and SoC values during t_2 to t_3 because of the absence of the master unit. Instead, the three DG units performed parallel operation with equal output powers, which fed approximately 400 W by the primary control with the same VRs. Meanwhile, the SoC values of these units decreased at different rates. At t_3, the communication of DG #1 was recovered. At t_4, SoC_2 re-followed SoC_1. However, the process for the coincidence of SoC_4 with SoC_1 was very slow. SoC_4 was unable to find a new average with the master unit until SoC_1 and SoC_2 reached their limits. Thus, an overcurrent inevitably appeared at t_5 when DGs #1 and #2 were shut down.

By contrast, with dynamic consensus algorithm, as long as the original edge weight constant ε is still within the convergence condition range of the remaining network, the stability can be maintained and a new convergence can be quickly found. As shown in Fig. 13, at t_2, DG #1 was disconnected from its neighbors DGs #2 and #3 in case of communication fault or intentional operation. The output power of DG #1 increased to 400 W by the primary control with basic VR as shown in Fig. 13. Meanwhile, the rest of the DG units quickly found a new SoC convergence in terms of the distributed DCA and continued to share the remaining load power, according to their ESS capacities and SoC values. At t_3, the communication of DG #1 was reconnected to DGs #2 and #3. After a short transient period, SoC_1, SoC_2, and SoC_3 were re-converged to a new average at t_4. Furthermore, the power outputs of the paralleled DG units were distributed according to the ESS capacities and SoC values again. The sudden change in output power during t_3 to t_4 is caused by the upper/lower saturation limits of PI controller in the SoC coordinated controller and the upper/lower limits of the VR deviations to prevent the potential inverter damage caused by overshoots and inrush of current during the reconnection process. At t_5, DGs #1, #2, and #3 simultaneously reached the SoC limit. No overcurrent appeared during this test. Thus, the proposed distributed DCA-based coordinated controller can achieve the balanced discharge rate control of ESS to improve the system reliability, and enhance the system flexibility, which includes the capacity of excluding and including online units.

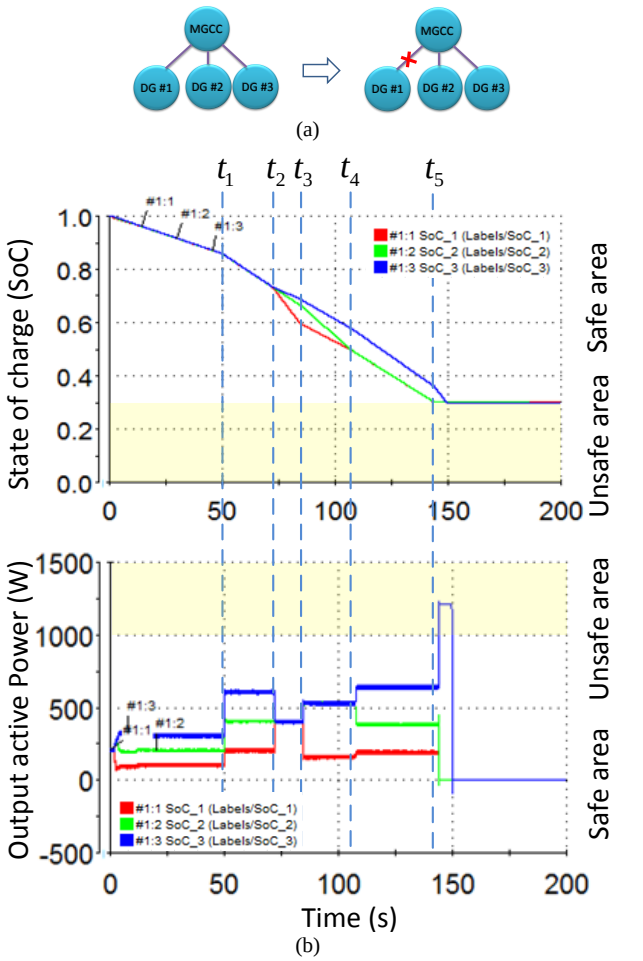

Fig. 12. Experimental results during communication fault of DG #1 with the centralized average method.

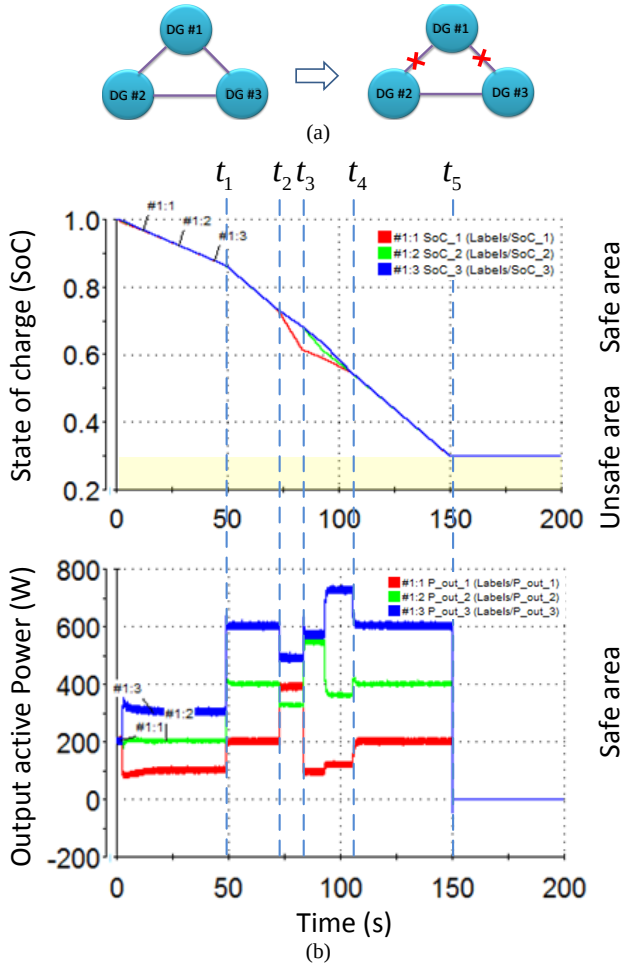

Fig. 13. Experimental results during communication fault of DG #1 with the proposed DCA-based coordinated control.

Given a large network consists of a number of nodes, which is beyond the experimental platform capability, simulations from a ten-node network in different scenarios were conducted to verify the control performance of the proposed control strategy in a large system.

D. Simulation results of the ten-node network with the proposed DCA-based SoC coordinated controller under a cross shape during communication fault

The transient response of a ten-node network under a cross shape during the communication fault of DG #1 is shown in Fig. 14. As shown in Fig. 14(a), before 5 s, the proposed DCA-based SoC coordinated control was not activated. The paralleled DG units equally share the load. At 5 s, the proposed control started to work. After about 15 s, the output power of each DG unit changed according to its ESS capacity. Meanwhile, the SoC values of these ten nodes decreased with a same gradient. At 50 s, an extra load is connected to the common bus. At 70 s, the communication links of DG #1 were suddenly disconnected from the system but its hardware remained connected and constantly operated. The power output of DG #1 was increased to 670 W by its primary control and basic *d*-axis VR. Meanwhile, given the distributed consensus algorithm, the other DG units quickly found a new SoC convergence and continued to share the remaining load power proportionally. At 80 s, after the communication of DG #1 was recovered, the system returned to the original convergence.

E. Simulation results of the ten-node network with the proposed DCA-based SoC coordinated controller changing from cross shape to ring shape

Fig. 15 shows the transient response of the ten-node network when its communication connection changes between a cross shape and a ring shape. The topologies are shown in Figs. 3(b) and (c). First, the ten-node network was connected in a cross shape. After a short period, the SoC values converged to a steady-state average value at approximately 20 s. At 50 s, a load step up change increased the power output of each DG unit. At 80 s, the communication links between DGs #1, #4, #6, and #9 were disconnected. Thus, the communication topology changed from a cross shape to a ring shape. At 120 s, these communication links were re-connected, which implies that the topology returned to the cross shape. It can be seen from Fig. 15, these changes did not influence the output power sharing and SoC values in the steady state. However, the cross or ring topology will affect the convergence time once a disturbance presents. More connections can provide faster convergence.

F. Simulation results of the ten-node network with the proposed DCA-based SoC coordinated controller during network separation

The transient response of a ten-node network in a ring shape

This article has been accepted for publication in a future issue of this journal, but has not been fully edited. Content may change prior to final publication. Citation information: DOI 10.1109/TSG.2017.2672882, IEEE Transactions on Smart Grid

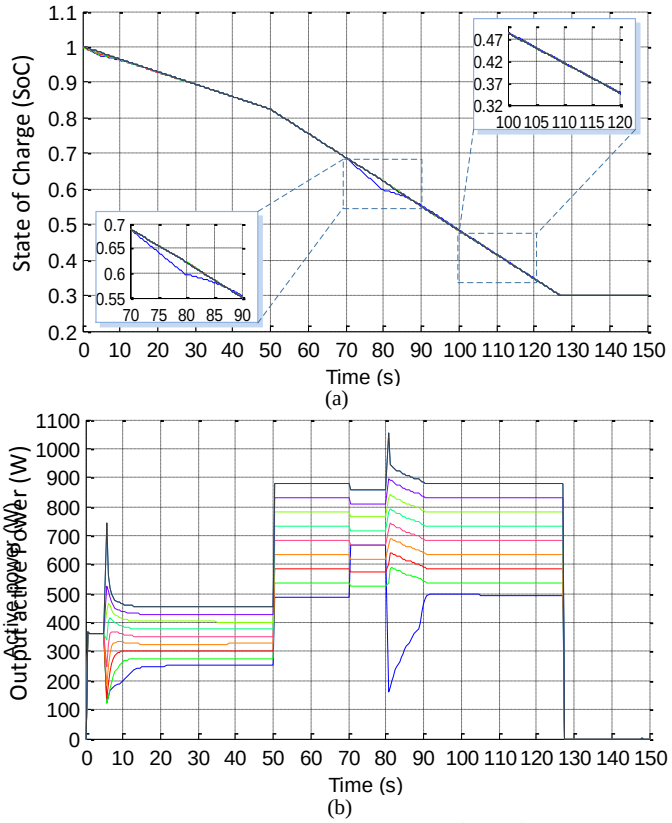

Fig. 14. Simulation results during communication fault of DG #1 with the proposed DCA-based coordinated control under cross shape. (a) SoC of ESSs. (b) Active power output of DGs.

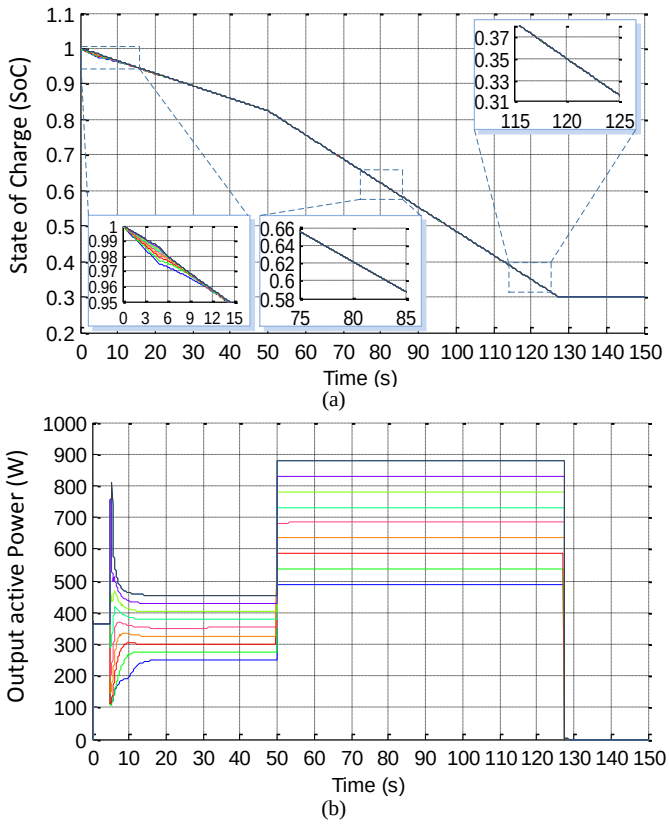

Fig. 15. Simulation results during topology change between cross and ring shapes with the proposed DCA-based coordinated control. (a) SoC of ESSs. (b) Active power output of DGs.

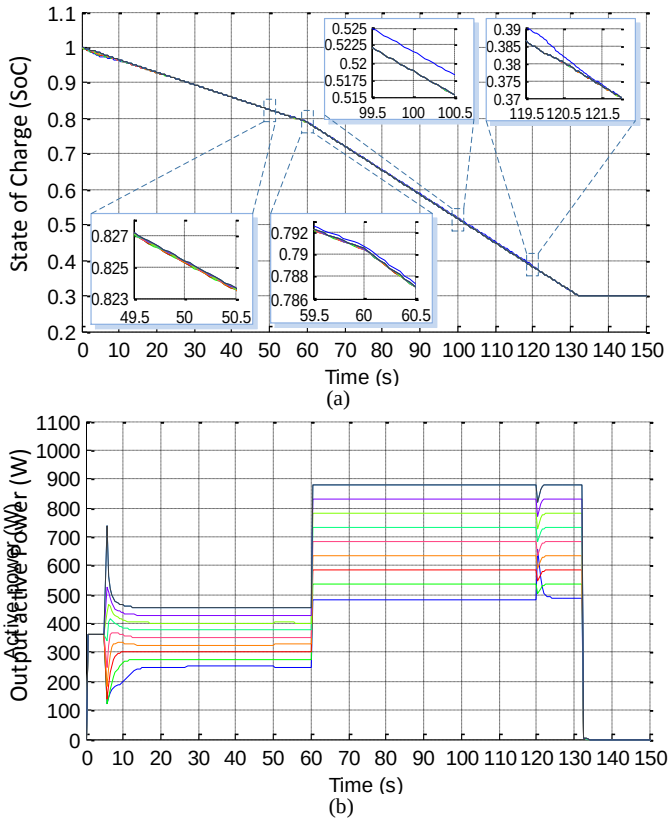

Fig. 16. Simulation results during network separation with the proposed DCA-based coordinated control. (a) SoC of ESSs. (b) Active power output of DGs.

during network separation is shown in Fig. 16. Initially, the communication links of these ten nodes are connected in a ring shape. After the proposed control is activated at 5 s, these ten DG units rapidly find an average SoC value. At 50 s, the communication links of DGs #1 and #10 were suddenly disconnected from the remaining DG units, but the hardware was still connected. The ten-node network is separated into two parts: one part contained eight nodes under an open ring shape; the other part included two nodes and only one communication link. As illustrated in Figs. 16(a) and (b), the change barely has no effect on the convergence result because separation occurred during the steady state. When a disturbance was presented, the convergence value changed. In this case, another resistive load was connected to the common bus at 60 s. The SoC values of the two sub-networks converged to two different average values according to the new network topologies. However, the small deviations between these two average values almost did not affect the power sharing ratio. At 120 s, the communication links were reconnected to a ring shape. As shown of the sub-figures in Fig. 16(a), the ten-node system re-converged to a global average value.

In summary, several improvements to the conventional power-sharing control and the droop-based centralized SoC coordinated control strategies are provided by the proposed DCA-based SoC controller. First, the proposed SoC-balancing control strategy is developed for AC MGs instead of DC MGs. Second, this approach can effectively avoid SPOF, thereby improving the system reliability and flexibility because of its distributed structure and robust communication network. Third, the approach effectively guarantees SoC balance to prevent

TABLE III
PERFORMANCE COMPARISON

	Existing Implementation	SoC rates balancing control capability	SPOF	Transient response	Robustness	Communication cost
Power-sharing control	AC/ DC MG	No	No	Slow/ Fast	Good	No
Centralized droop-based SoC rates balancing control	DC MG	Yes	Yes	Slow	Poor	More
Decentralized droop-based SoC rates balancing control	DC MG	Yes	No	Slow	Poor	Less
Proposed SoC rates balancing control	AC MG	Yes	No	Fast	Good	Less

overcurrent incidents and DGs of unintentional outages in an AC MG. Fourth, the method provides a faster transient response and decoupled output-current-sharing because of the autonomous current-sharing control at the primary level. Fifth, the controller presents a lower sensitivity with respect to the secondary control level parameters over the system dynamics caused by the larger stability margin of the primary controller. The advantages and disadvantages of the proposed strategy compared with the other methods are summarized in Table III.

VI. CONCLUSIONS

A DCA-based coordinated secondary control with an autonomous current sharing control strategy was proposed in this paper for the balanced discharge rate of ESSs in islanded AC MGs. Compared with previously proposed methods, this approach can ensure a balanced discharge rate among DGs to provide higher reliability, expandability, and flexibility. In addition, the approach achieves various improvements, such as a faster response, more accurate output current sharing, and a larger stability margin. Root loci for an *n*-DG network in the *z*-domain from a discrete state-space model with the proposed SoC coordinated controller show low sensitivity to control parameters over the system dynamics. Finally, the simulation and experimental results in various scenarios verify the effectiveness and flexibility of the proposed controller.

REFERENCES

[1] R. H. Lasseter and P. Paigi, "Microgrid: A conceptual solution," *in Proc. IEEE PESC*, Aachen, Germany, 2004, pp. 4285-4290.

[2] Vasquez, J.C., Guerrero, J.M., Luna, A., Rodriguez, P., "Adaptive Droop Control Applied to Voltage-Source Inverters Operating in Grid-Connected and Islanded Modes," *Industrial Electronics, IEEE Transactions on*, vol. 56, no. 10, 4088-4096, Oct. 2009.

[3] J. Guerrero, L. de Vicuna, J. Matas, M. Castilla, and J. Miret, "A wireless controller to enhance dynamic performance of parallel inverters in distributed generation system," *IEEE Trans. Power Electron.*, vol. 19, no. 5, pp. 1205–1213, Sep. 2004.

[4] K. Jong-Yul, J. Jin-Hong, K. Seul-Ki, C. Changhee, P. June-Ho, K. Hak- Man, and N. Kee-Young, "Cooperative control strategy of energy storage system and microsources for stabilizing the microgrid during islanded operation," *IEEE Trans. Power Electron*., vol. 25, no. 12, pp. 3037–3048, Dec. 2010.

[5] S. Adhikari and F. Li, "Coordinated V-f and P-Q control of solar photovoltaic generators with MPPT and battery storage in microgrids," *IEEE Trans. Smart Grid*, vol. 5, no. 3, pp. 1270–1281, May 2014.

[6] H. Bode, *Lead Acid Batteries*. New York: Wiley, 1977.

[7] M. A. Casacca and Z. M. Salameh, "Determination of lead-acid battery capacity via mathematical modeling techniques," *IEEE Trans. Energy Convers.*, vol. 7, no. 3, pp. 442–446, 1992.

[8] Y.-K. Chen, Y.-C. Wu, C.-C. Song, and Y.-S. Chen, "Design and implementation of energy management system with fuzzy control for DC microgrid systems," *IEEE Trans. Power Electron*., vol. 28, no. 4, pp. 1563–1570, Apr. 2013.

[9] Guerrero, J.M., Chandorkar, M., Lee, T., Loh, P.C., "Advanced Control Architectures for Intelligent Microgrids—Part I: Decentralized and Hierarchical Control," *Industrial Electronics, IEEE Transactions on*, vol.60, no.4, pp.1254-1262, April 2013.

[10] Y. Guan, J. M. Guerrero, J. C. Vasquez. "Coordinated secondary control for balanced discharge rate of energy storage system in islanded microgrids," *Power Electronics and ECCE Asia (ICPE-ECCE Asia), 2015 International Conference on*, 1-5 June 2015, Seoul, PP. 475-481.

[11] X. Lu, K. Sun, Guerrero, J.M. Vasquez, J.C. L. Huang, "State-of-Charge Balance Using Adaptive Droop Control for Distributed Energy Storage Systems in DC Microgrid Applications," *Industrial Electronics, IEEE Transactions on*, vol.61, no.6, pp.2804-2815, June. 2014

[12] T. Dragicevic, J. Guerrero, J. Vasquez, and D. Skrlec, "Supervisory control of an adaptive-droop regulated DC microgrid with battery management capability," *IEEE Trans. Power Electron*., vol. 29, no. 2, pp. 695–706, Feb. 2013.

[13] Kakigano, H.; Miura, Y.; Ise, T., "Distribution Voltage Control for DC Microgrids Using Fuzzy Control and Gain-Scheduling Technique," *Power Electronics, IEEE Transactions on*, vol.28, no.5, pp.2246-2258, May 2013.

[14] Chendan Li, Dragicevic, T., Diaz, N.L., Vasquez, J.C., Guerrero, J.M., "Voltage scheduling droop control for State-of-Charge balance of distributed energy storage in DC microgrids," *Energy Conference (ENERGYCON), 2014 IEEE International*, 13-16 May 2014, Cavtat, pp: 1310-1314.

[15] Chendan Li, Garcia Plaza, M., Andrade, F., Vasquez, J.C., Guerrero, J.M., "Multiagent based distributed control for state-of-charge balance of distributed energy storage in DC microgrids," *Industrial Electronics Society, IECON*, Oct. 29 2014-Nov. 1 2014, Dallas, pp: 2180 – 2184.

[16] Diaz, N.L., Dragicevic, T., Vasquez, J.C., Guerrero, J.M. "Intelligent Distributed Generation and Storage Units for DC Microgrids—A New Concept on Cooperative Control Without Communications Beyond Droop Control," *Smart Grid, IEEE Transactions on*, vol. 5, no. 5, pp: 2476 – 2485, Sept. 2014.

[17] N. L. Diaz, T. Dragicevic, J. C. Vasquez, J. M. Guerrero. "Fuzzy-logic-based gain-scheduling control for state-of-charge balance of distributed energy storage systems for DC microgrids," *Applied Power Electronics Conference and Exposition (APEC), 2014 Annual IEEE*, 16-20 Mar. 2014, Fort Worth, TX, pp.: 2171 - 2176.

[18] R. Olfati-Saber, J. A. Fax, and R. M. Murray, "Consensus and cooperation in networked multi-agent systems," *Proceedings of the IEEE*, vol. 95, no. 1, pp. 215–233, Jan. 2007.

[19] Kriegleder, M., Oung, R.. D'Andrea, R., "Asynchronous implementation of a distributed average consensus algorithm," *Intelligent Robots and Systems (IROS), 2013 IEEE/RSJ International Conference on*, vol., no., pp.1836-1841, 3-7 Nov. 2013

[20] D. Spanos, R. Olfati-Saber, and R. Murray, "Dynamic consensus for mobile networks," *in IFAC World Congress*, 2005.

[21] M. Kriegleder, "A Correction to Algorithm A2 in "Asynchronous Distributed Averaging on Communication Networks"," *IEEE/ACM Transactions on Networking*, vol.22, no. 6, pp. 2026- 2027, Dec. 2014.

[22] Y. A. Ibrahim Mohamed, E. F. El-Saadany. "Adaptive Decentralized Droop Controller to Preserve Power Sharing Stability of Paralleled Inverters in Distributed Generation Microgrids," *IEEE Transactions on Power Electronics*, vol. 23, no. 6, pp.2806-2816, Nov. 2008

[23] Yajuan Guan, Vasquez, J.C., Guerrero, J.M., Alves Coelho, E.A. "Small-signal modeling, analysis and testing of parallel three-phase-inverters with a novel autonomous current sharing controller," *Applied Power Electr. Conf. and Expo. (APEC)*, 2015 IEEE, pp. 571 – 578, Charlotte, NC, 15-19 Mar. 2015.

[24] N. Pogaku, M. Prodanovic, and T. C. Green, "Modeling, analysis and testing of autonomous operation of an inverter-based microgrid," *IEEE Trans. Power Electron*., vol. 22, no. 2, pp. 613–625, Mar. 2007.
[25] Meng, L., Dragicevic, T., Roldan-Perez, J., Vasquez, J.C., Guerrero, J.M., "Modeling and Sensitivity Study of Consensus Algorithm-Based Distributed Hierarchical Control for DC Microgrids," *Smart Grid, IEEE Transactions on*, vol., no.99, pp., May. 2015.
[26] Guan, Y., Guerrero, J.M., Zhao, X., Vasquez, J.C., Guo, X. "A New Way of Controlling Parallel-Connected Inverters by Using Synchronous-Reference-Frame Virtual Impedance Loop—Part I: Control Principle," *Power Electronics, IEEE Transactions on*, vol. 31, no. 6, pp: 4576 - 4593, June. 2016.
[27] L. Xiao and S. Boyd, "Fast linear iterations for distributed averaging," *in Proc. 42nd IEEE Int. Conf. Decis. Control*, vol. 5. Maui, HI, USA, 2003, pp. 4997–5002.
[28] A. Kaveh. Optimal Analysis of Structures by Concepts of Symmetry and Regularity, *Springer-Verlag Wien*, 2013.
[29] Shafiee, Q., Guerrero, J.M., Vasquez, J.C., "Distributed Secondary Control for Islanded Microgrids—A Novel Approach," *Power Electronics, IEEE Transactions on*, vol. 29, No. 2, pp, 1018 – 1031, Feb. 2014.
[30] Shafiee, Q., Stefanovic, C., Dragicevic, T., Popovski, P., Vasquez, J.C., Guerrero, J.M., "Robust Networked Control Scheme for Distributed Secondary Control of Islanded Microgrids," *Industrial Electronics, IEEE Transactions on*, vol. 61, no. 10, pp. 5363 – 5374, Oct. 2014.
[31] R. Olfati-Saber, "Ultrafast consensus in small-world networks," Proceedings of the 2005, American Control Conference, June 2005, vol. 4, pp. 2371 – 2378.

Yajuan Guan (S'14 M'16) received the B.S. degree and M.S. degree in electrical engineering from the Yanshan University, Qinhuangdao, Hebei, China, and the Ph.D. degree in power electronics from the Aalborg University, Aalborg, Denmark, in 2007, 2010 and 2016 respectively. From 2010 to 2012, she was an Assistant Professor in Institute of Electrical Engineering (IEE), Chinese Academy of Sciences (CAS). Since 2013, she has been a Lecturer in IEE; CAS. She is currently a Postdoctoral Fellow with Aalborg University, Aalborg, Denmark, as part of the Denmark Microgrids Research Programme (www.microgrids.et.aau.dk).

Her research interests include microgrids, distributed generation systems, power converter for renewable energy generation systems, and ancillary services for microgrids.

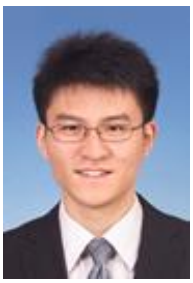

Lexuan Meng (S'13–M'15) received the B.S. degree in Electrical Engineering and M.S. degree in Electrical Machine and Apparatus from Nanjing University of Aeronautics and Astronautics (NUAA), Nanjing, China, in 2009 and 2012, respectively. In 2015, he received the Ph.D. degree in Power Electronic Systems from Department of Energy Technology, Aalborg University, Denmark. He is currently a post-doctoral researcher in the same department working on flywheel energy storage and onboard electric power systems.

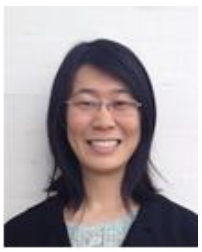

Chendan Li (S'13) received the B.S. degree in Electrical Engineering from Nanjing Agricultural University, in 2009, M.S. degree in Nanjing Univ. of Aeronautics& Astronautics, in 2012, Nanjing, Jiangsu, China, and PhD degree from Aalborg University, Aalborg, Denmark, in 2016.

Her main research interests include steady state and dynamic analysis, optimization and distributed control for AC and DC microgrid, information and communications technology (ICT) and data analysis for microgrids.

Juan C. Vasquez (M'12-SM'14) received the B.S. degree in electronics engineering from the Autonomous University of Manizales, Manizales, Colombia, and the Ph.D. degree in automatic control, robotics, and computer vision from the Technical University of Catalonia, Barcelona, Spain, in 2004 and 2009, respectively. He was with the Autonomous University of Manizales, where he taught courses on digital circuits, servo systems, and flexible manufacturing systems. He was also with the Technical University of Catalonia, as a Post-Doctoral Assistant, teaching courses based on renewable energy systems. In 2011, he was Assistant Professor in microgrids and currently he is working as an Associate Professor at the Department of Energy Technology, Aalborg University, Denmark. Dr. Vasquez is the co-responsible of the Research Program in Microgrids. From Feb. 2015 to April. 2015 he was a Visiting Scholar at the Center of Power Electronics Systems (CPES) at Virginia Tech.

His current research interests include operation, power management, hierarchical control, optimization and power quality applied to distributed generation and ac/dc microgrids. Dr. Vasquez is currently a member of the IEC System Evaluation Group SEG4 on LVDC Distribution and Safety for use in Developed and Developing Economies and the Renewable Energy Systems Technical Committee TC-RES in IEEE Industrial Electronics Society.

Josep M. Guerrero (S'01-M'04-SM'08-FM'15) received the B.S. degree in telecommunications engineering, the M.S. degree in electronics engineering, and the Ph.D. degree in power electronics from the Technical University of Catalonia, Barcelona, in 1997, 2000 and 2003, respectively. Since 2011, he has been a Full Professor with the Department of Energy Technology, Aalborg University, Denmark, where he is responsible for the Microgrid Research Program. From 2012 he is a guest Professor at the Chinese Academy of Science and the Nanjing University of Aeronautics and Astronautics; from 2014 he is chair Professor in Shandong University; and from 2015 he is a distinguished guest Professor in Hunan University.

His research interests is oriented to different microgrid aspects, including power electronics, distributed energy-storage systems, hierarchical and cooperative control, energy management systems, and optimization of microgrids and islanded minigrids. Prof. Guerrero is an Associate Editor for the IEEE TRANSACTIONS ON POWER ELECTRONICS, the IEEE TRANSACTIONS ON INDUSTRIAL ELECTRONICS, and the IEEE Industrial Electronics Magazine, and an Editor for the IEEE TRANSACTIONS on SMART GRID and IEEE TRANSACTIONS on ENERGY CONVERSION. He has been Guest Editor of the IEEE TRANSACTIONS ON POWER ELECTRONICS Special Issues: Power Electronics for Wind Energy Conversion and Power Electronics for Microgrids; the IEEE TRANSACTIONS ON INDUSTRIAL ELECTRONICS Special Sections: Uninterruptible Power Supplies systems, Renewable Energy Systems, Distributed Generation and Microgrids, and Industrial Applications and Implementation Issues of the Kalman Filter; and the IEEE TRANSACTIONS on SMART GRID Special Issue on Smart DC Distribution Systems. He was the chair of the Renewable Energy Systems Technical Committee of the IEEE Industrial Electronics Society. In 2014 he was awarded by Thomson Reuters as Highly Cited Researcher, and in 2015 he was elevated as IEEE Fellow for his contributions on "distributed power systems and microgrids."